Electrochimica Acta 513 (2025) 145558

Contents lists available at ScienceDirect

Electrochimica Acta

journal homepage: www.journals.elsevier.com/electrochimica-acta

Influence of binaphthalene moiety on properties of poly(arylene pyridine) membranes for high temperature polymer electrolyte membrane fuel cells

Yao Lu [a], Zhejing Zhang [a], Lele Wang [a], Qian Wang [a], Jin Wang [b,*], Jingshuai Yang [a,*]

[a] Department of Chemistry, College of Sciences, Northeastern University, Shenyang 110819, PR China
[b] College of Pharmacy, Shenyang Medical College, Shenyang 110034, PR China

ARTICLE INFO

Keywords:
High-temperature proton exchange membranes
Poly(arylene pyridine)
Fuel cell

ABSTRACT

High temperature proton exchange membranes (HT-PEMs) are vital components in HT-PEM fuel cells (HT-PEMFCs). While phosphoric acid (PA) doped polybenzimidazole (PBI) membranes are commonly used in these fuel cells, their synthesis is complex and requires carcinogenic monomers. Therefore, developing cost-effective and easily prepared HT-PEMs with adequate physicochemical properties and high fuel cell performance is highly important. In this study, we synthesize binaphthalene based poly(arylene pyridine)s using a straightforward Friedel-Crafts reaction involving 1,1′-binaphthalene and 4-acetylpyridine (or 4-pyridinecarboxaldehyde). The resulting PBNP-CH_3 membrane exhibits an excellent PA absorption capability, meanwhile maintaining improved dimensional and mechanical stabilities due to the rigid and planar of binaphthyl units. By immersing the PBNP-CH_3 membrane in 85 wt% PA at 30 °C, it obtains a PA uptake of 252.9 %, a high tensile strength of 7.2 MPa, and a good conductivity of 73.2 mS cm^{-1} at 180 °C. Consequently, at 200 °C without backpressure, a H_2-O_2 fuel cell equipped with the PBNP-CH_3/252.9 %PA membrane reaches a peak power density of 1047 mW cm^{-2}, indicating significant potential for use in HT-PEMFCs.

1. Introduction

The increasing reliance on conventional fossil fuels has led to significant environmental degradation, highlighting the urgent need for clean, renewable energy sources and efficient energy conversion technologies [1,2]. Proton exchange membrane fuel cells (PEMFCs), known for their high efficiency and cleanliness, have garnered growing interest [3–5]. However, conventional PEMFCs typically operate at temperatures below 100 °C, which can result in slower electrode kinetics, complex thermo-water management, and a heightened risk of CO poisoning [6,7]. In contrast, high temperature PEMFCs (HT-PEMFCs) operating above 100 °C offer several advantages, including enhanced electrode reaction kinetics, particularly for the oxygen reduction reaction (ORR) [7], improved resistance to CO poisoning at the electrodes, and simpler hydrothermal management systems [8,9].

The central component of these systems, the high temperature proton exchange membrane (HT-PEM), presents unique challenges [6,10]. Traditional perfluorosulfonic acid polymer membranes like Nafion are unsuitable for use above 100 °C due to their dependence on water for proton conduction [11]. Additionally, their manufacturing process is complex and costly. Most research has focused on HT-PEMs doped with non-volatile inorganic acids like phosphoric acid (PA) [12–14], which exhibits excellent proton conductivity [15]. Polybenzimidazole (PBI) membranes were initially proposed for HT-PEMFCs by Wainright and co-workers [16] and are now considered viable for commercial applications. Since then, various modifications and derivatives of PBI have been explored [8,17–20]. For example, Jana et al. developed a novel monomer of 2,6-bis(3′,4′-diaminophenyl)−4-phenylpyridine instead of the traditional monomer of 3,3′,4,4′-tetraaminobiphenyl (TBA) and synthesized various PBI polymers with different variant structure, which displayed improved performance [21–25]. In addition, to achieve PBI/PA membranes with enhanced mechanical strength and oxidative resistance, it is essential for PBI to have relatively high molecular weights [26]. However, high-molecular-weight PBI polymers often suffer from poor solubility in conventional organic solvents [18–20,26,27]. Moreover, the production of the TBA monomer used in PBI synthesis poses carcinogenic risks. Consequently, there is significant interest in developing new HT-PEMs that offer excellent proton conductivity, robust mechanical strength, and superior thermal stability.

In recent years, a variety of polymers with diverse structural designs have emerged as potential alternatives to PBI. For example, poly(arylene ether sulfone/ketone)s and poly(vinyl chloride) grafted with

* Corresponding authors.
E-mail addresses: wangjin@symc.edu.cn (J. Wang), yjs@mail.neu.edu.cn (J. Yang).

https://doi.org/10.1016/j.electacta.2024.145558
Received 29 October 2024; Received in revised form 14 December 2024; Accepted 21 December 2024
Available online 22 December 2024

imidazolium or quaternary ammonium (QA) cations have been suggested as candidate HT-PEMs [8,28–30]. Despite their superior ability to accommodate PA doping, QA side-chain grafted HT-PEMs often exhibit insufficient chemical and mechanical stability [26], which reduces fuel cell lifespan. Interestingly, aromatic polymers with main-chain N-heterocyclic groups have been proposed as HT-PEMs due to their exceptional mechanical and chemical stability. For instance, Kallitsis and colleagues synthesized several aromatic polyether polymers featuring pyridine groups along the main chains [31,32].

Polyhydroxyalkylation reactions between electron-rich arenes and ketones or aldehydes represent an effective polymerization approach that can be performed using superacid-catalyzed chemistry [33]. Zolotukhin et al. employed these synthetic routes to produce various rigid, wholly aromatic, ether-bond-free polymers [34–36]. Building on these pioneering works, our group has synthesized a range of polymers containing N-heterocyclic groups for HT-PEMFCs, including those with piperidine [12], imidazole [28], and pyridine [37] groups. Among these polymers, poly(arylene pyridine)s demonstrated excellent chemical stability due to their fully aromatic backbones and π-conjugated pyridine rings. Furthermore, both poly(*p*-terphenyl-*co*-4-acetylpyridine) (PTAP) and poly(biphenyl-*co*-4-acetylpyridine) (PBAP) membranes, characterized by triarylmethane-like backbones and basic pyridine groups, exhibited remarkable PA doping capabilities [37]. The PBAP membrane achieved a PA uptake of 350 % when immersed in a 50 wt% PA solution at 30 °C, and it even dissolved in an 85 wt% PA solution, necessitating blending with reinforcing materials to improve mechanical stability. For instance, poly(ether ketone cardo) (PEKC), a commercial engineering thermoplastic, has been utilized to enhance the mechanical and dimensional stability of PBAP-based membranes [38]. Consequently, the H_2—O_2 HT-PEMFC utilizing the PBAP-50 %PEKC/170 %PA membrane at 160 °C attained a peak power density of 632 mW cm^{-2}.

It is widely recognized that introducing rigid and bulky moieties into polymer backbones significantly impacts membrane properties. Binaphthalene, a naphthalene derivative known for its luminescent properties, has recently garnered considerable attention in the realm of anion exchange membranes (AEMs) [39,40]. Unlike linear biphenyl, the dinaphthyl group has a distorted dihedral angle of 74° between its two naphthyl planes due to steric hindrance [39,41], which is larger than the approximately 45° angle observed in biphenyl. This bulky and twisted structure enhances the free volume within AEMs, leading to improved ionic conductivity. For example, Li et al. synthesized poly(binaphthyl-*co*-terphenyl quinuclidinium)-based AEMs, achieving an OH^- conductivity of 170.21 mS cm^{-1} at 80 °C [40]. While substantial research has focused on AEMs incorporating binaphthalene functionalities, the application of this unique structure in HT-PEMs remains largely unexplored. This gap presents an opportunity for further exploration into the development and optimization of binaphthalene-based poly(arylene pyridine)s for HT-PEMs.

In this study, we expand upon our previous work on PTAP [37] by incorporating the bulky and twisted dinaphthyl structure into pyridine-based polymers through Friedel-Crafts hydroxyalkylation reactions. Two pyridine derivatives, namely 4-acetylpyridine and 4-pyridinecarboxaldehyde, were employed as monomers for polymerization with binaphthalene. To investigate the structure-property relationships and evaluate the impact of the dinaphthyl structure on membrane properties, we synthesized two reference polymers by replacing the binaphthalene monomer with biphenyl. The physicochemical characteristics and fuel cell performance of the new membranes, which incorporate dinaphthyl and pyridine units, are anticipated to demonstrate exceptional performance, offering a novel strategy to enhance the properties of polymer electrolytes HT-PEMFCs.

2. Experimental

2.1. Materials

Biphenyl (BP), 1,1′-binaphthalene (BNP), 4-pyridinecarboxaldehyde, trifluoroacetic acid (TFA), methanesulfonic acid (MSA), and trifluoromethanesulfonic acid (TFSA) were supplied by Adamas Reagent Ltd. Additionally, 4-acetylpyridine was sourced from Energy Chemical. Other reagents included dichloromethane (CH_2Cl_2), sodium bicarbonate ($NaHCO_3$), dimethyl sulfoxide (DMSO), *N*-methylpyrrolidone (NMP), and an 85 wt% phosphoric acid (PA) solution. None of these chemicals were subjected to purification prior to use.

2.2. Synthesis of the polymers

The polymers including PBP-CH_3, PBNP-CH_3, PBP-H, and PBNP-H were synthesized using a modified version of our previous studies [42]. Taking PBNP-CH_3, as an example, under ice bath conditions, added 1.000 g (3.9318 mmol) of 1,1′-binaphthyl into a 50 mL two-necked flask, followed by 5 mL of CH_2Cl_2. Once the solid powder was mostly dissolved, added 0.6221 g (5.1354 mmol) of 4-acetylpyridine into the flask, and stirred the mixture evenly using mechanical stirring. Slowly added 4 mL of TFSA, and allowed the reaction to proceed for 1 hour in the ice bath. After removing the ice bath, the reaction was continued at room temperature for 24 h, obtaining a purple-black viscous solution. Poured the mixture into 1 M $NaHCO_3$ solution to yield a brown fibrous polymer, followed by soaking it in the alkaline solution for 24 h to fully neutralize the acid. The polymer was washed repeatedly with deionized water until neutral, then placed in a vacuum oven to dry at 80 °C for 24 h, yielding the polymer of PBNP-CH_3. Fig. 1 illustrates the chemical structure and the synthesis process of various polymers.

2.3. Membrane casting

Membranes were fabricated using a solution-casting method. A 2.0 wt% polymer solution was prepared by dissolving each polymer in the solvent at 80 °C. Specifically, PBP-CH_3 and PBNP-CH_3 were dissolved in NMP, while PBP-H and PBNP-H were dissolved in DMSO with TFA. Once homogeneous solutions were achieved, they were cast onto Petri dishes. The solvent was evaporated at 80 °C in an oven until fully removed. The membranes were then peeled from the dishes and thoroughly rinsed with deionized water. Finally, each membrane was dried at 100 °C and then the uniform and transparent membrane was obtained.

2.4. Acid doping and swelling

After drying, the membranes were immersed in 75 wt% and 85 wt% PA solutions at 30 °C until a constant mass was reached. Any residual PA on the surface was removed using filter paper. The PA doped membranes were then dried in a vacuum oven at 100 °C to eliminate water, after which their weight and dimensions were promptly measured. The acid doping content (ADC%) of each membrane was calculated based on the mass difference before and after PA doping using Eq. (1). The degrees of swelling, including area swelling (S%) and volume swelling (V%), were calculated from the dimensional changes before and after the PA doping process using Eqs. (2) and (3):

$$ADC\Big/\% = \frac{M_{PA} - M_0}{M_0} \times 100\% \tag{1}$$

$$S\Big/\% = \frac{S_{PA} - S_0}{S_0} \times 100\% \tag{2}$$

$$V\Big/\% = \frac{V_{PA} - V_0}{V_0} \times 100\% \tag{3}$$

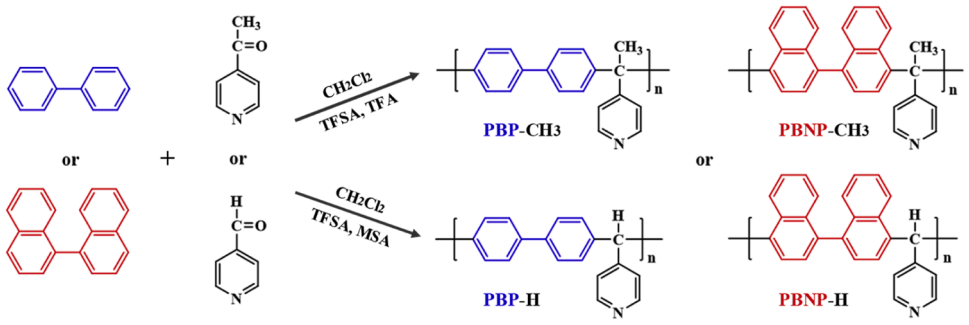

Fig. 1. Synthesis of PBP-CH_3, PBNP-CH_3, PBP-H and PBNP-H copolymers.

In Eq. (1), M_{PA} is the mass of the membrane after PA doping, while M_0 is the mass of the pristine membrane. Variables S_{PA} and S_0 represent the membrane areas before and after immersion in the PA solution, as per Eq. (2). Similarly, V_{PA} and V_0 correspond to the volume measurements in Eq. (3).

2.5. Characterizations

The inherent viscosity (η) of the polymers was measured at 30 °C using a Ubbelohde-type capillary viscometer, with polymer solutions prepared at a concentration of 100 mg dL^{-1}. Each polymer solution underwent three replicate measurements, and η was calculated using Eq. (4) [37,43]:

$$\eta = \ln\left(\frac{t_s}{t_0}\right) \Big/ c \tag{4}$$

where t_s is the efflux time of the polymer solution, and t_0 is the efflux time of the pure solvent.

Proton nuclear magnetic resonance (^{1}H NMR) spectra were obtained using a Bruker AVANCE 600 MHz spectrometer, with tetramethylsilane (TMS) as the internal standard and deuterated chloroform ($CDCl_3$) as the solvent. Fourier transform infrared (FT-IR) spectra were recorded using a Bruker VERTEX70 spectrometer. Surface images of the membranes were analyzed using a scanning electron microscope (SEM, SU-8010), with samples coated with platinum under vacuum conditions.

Thermogravimetric analysis (TGA) was performed using a Mettler Toledo TGA/DSC^{3+} instrument under a nitrogen atmosphere, with a heating rate of 10 °C min^{-1}. The oxidative stability of the membranes was assessed using the Fenton test [28,30], which involved immersing membrane samples in Fenton's reagent containing 3 wt% H_2O_2 and 4.0 ppm Fe^{2+} (supplied by adding $(NH_4)_2Fe(SO_4)_2{\cdot}6H_2O$) at 68 °C. After predetermined intervals, the samples were rinsed with distilled water and dried in an oven at 80 °C until their weight stabilized. Fresh Fenton's reagent was prepared for each repeat test.

Mechanical properties were evaluated using a tensile testing machine (CMT2000, SHIJIN Company, China) at room temperature, with a constant separating speed of 5 mm min^{-1}. Membrane samples were shaped into dumbbells, with the middle section measuring 25 mm in length and 4 mm in width.

Anhydrous proton conductivity of the PA-doped membranes was measured using a four-probe conductivity cell at a frequency of 4 kHz [44]. To minimize moisture influence, membrane samples were preheated at 100 °C for approximately 1 hour prior to conductivity measurements. The measurements were conducted in an oven without humidification under ambient air. The oven temperature was increased from 100 °C to 180 °C, recording the resistance (R) of the membrane at 10 °C increments. Proton conductivity (σ) was calculated using the following equation:

$$\sigma = \frac{L}{RS} \tag{5}$$

where L is the distance between the electrodes, S is the cross-sectional area of the membrane, and R is the measured resistance.

2.6. Fuel cell performance

Gas diffusion electrodes (GDEs) were prepared by spraying an ink containing 60 % Pt/C catalyst dispersed in ethanol onto carbon papers to form the catalyst layer. The loadings of the Pt/C catalyst and the PBI binder were 0.7 mg cm^{-2} and 0.07 mg cm^{-2}, respectively. Membrane electrode assemblies (MEAs) were fabricated by hot-pressing two GDEs onto a PA-doped membrane at 140 °C under a pressure of 70 kg cm^{-2} for 2.5 minutes, resulting in an MEA with an active area of 4.0 cm^2 (2.0 cm × 2.0 cm). The performance of the single H_2—O_2 fuel cell was evaluated over a temperature range of 120 °C to 200 °C, with H_2 supplied at a rate of 120 mL min^{-1} and O_2 at 60 mL min^{-1} at atmospheric pressure, without humidification [45].

3. Results and discussions

3.1. Synthesis of polymers and fabrication of membranes

In this study, we designed a series of robust, fully aromatic polymers without ether linkages that incorporate pyridine units through Friedel-Crafts polymerization reactions involving acetylpyridine or pyridylaldehyde with biphenyl or 1,1′-binaphthalene, as illustrated in Fig. 1. The inherent viscosities of PBP-CH_3, PBNP-CH_3, PBP-H, and PBNP-H were measured to be 0.54 dL g^{-1}, 1.06 dL g^{-1}, 0.27 dL g^{-1}, and 0.66 dL g^{-1}, respectively, at a polymer concentration of 0.1 g dL^{-1} in NMP. These results indicate that the 1,1′-binaphthalene monomer exhibited greater reactivity than biphenyl, leading to higher viscosities for PBNP-CH_3 and PBNP-H compared to PBP-CH_3 and PBP-H. It is well known that a polymer's viscosity significantly impacts the mechanical properties of the corresponding membrane; generally, higher polymer viscosity correlates with increased tensile strength. Thus, membranes featuring the dinaphthyl structure are particularly attractive for use as HT-PEMs.

Regarding solubility, the polymers derived from 4-acetylpyridine (namely, PBP-CH_3 and PBNP-CH_3) displayed good solubility in NMP and $CHCl_3$ but were insoluble in DMSO. In contrast, the polymers derived from 4-pyridinecarboxaldehyde, PBP-H and PBNP-H, exhibited good solubility in DMSO when TFA was added, yet were insoluble in $CHCl_3$. Using the solution-casting method with NMP or DMSO as solvents, we successfully obtained four pure and transparent membranes: PBP-CH_3, PBNP-CH_3, PBP-H, and PBNP-H. As shown in Fig. 2, the PBP-CH_3 and PBNP-CH_3 membranes appeared brown, while the PBP-H and PBNP-H membranes exhibited a light yellow color. Furthermore, Fig. 2 includes SEM micrographs, which reveal that all membranes possessed dense and impermeable structures, advantageous for gas separation in fuel cell systems [26,46].

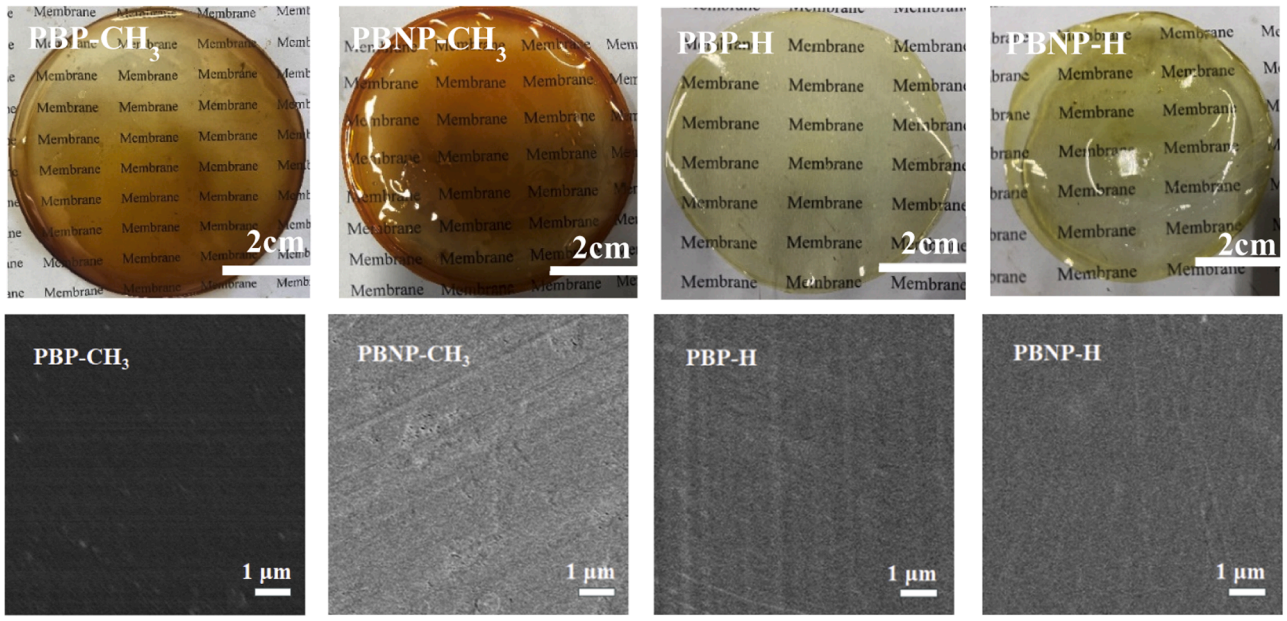

Fig. 2. Photographic and SEM images of PBP-CH_3, PBNP-CH_3, PBP-H and PBNP-H membranes.

3.2. ^{1}H NMR and FT-IR spectra

The chemical structures of the synthesized polymers were verified using ^{1}H NMR spectroscopy. As shown in Fig. 3, the methyl proton signals (peak 1) appeared at 2.2 ppm for PBP- CH_3 and 2.4 ppm for PBNP- CH_3 [37]. In contrast, PBP-H and PBNP-H exhibited a distinct characteristic peak at 6.1 ppm (peak 1′), corresponding to the –CH group. Compared to the biphenyl-based polymers (PBP-CH_3 and PBP-H), the dinaphthyl-based polymers display additional peaks in the range of 7.0–8.5 ppm, which correspond to the aromatic protons of the dinaphthyl units. These ^{1}H NMR results confirm the successful synthesis of all four polymers.

FT-IR spectroscopy was also employed to characterize the chemical structures of the PBP-CH_3, PBNP-CH_3, PBP-H, and PBNP-H membranes. As illustrated in Fig. 4, the bending vibrations of the aromatic C—H groups were observed between 752 and 885 cm^{-1} [37,45]. Additionally, the absorption band at 3035 cm^{-1} indicated the stretching vibrations of the aromatic C–H bonds. A distinct absorption peak at 2917 cm^{-1} was attributed to the stretching vibrations of the aliphatic C—H bonds. Moreover, characteristic absorption bands of the pyridine rings were noted at 1583 cm^{-1} and 1667 cm^{-1}, corresponding to the C = C and C = N bonds, respectively. Therefore, the infrared spectra further confirm the successful synthesis of the PBP-CH_3, PBNP-CH_3, PBP-H, and PBNP-H polymers.

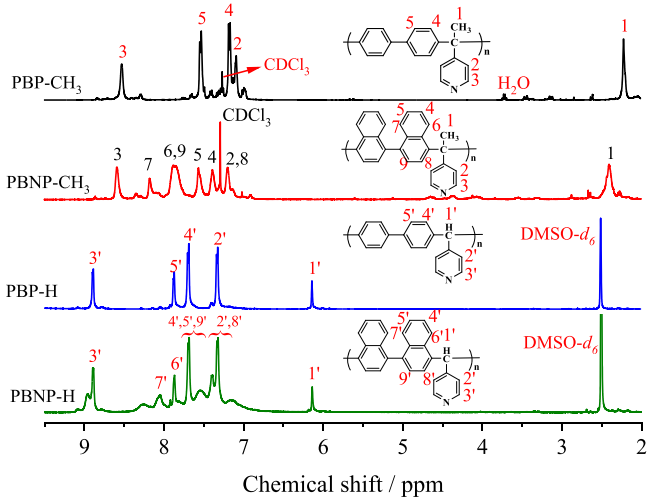

Fig. 3. ^{1}H NMR spectra of PBP-CH_3, PBNP-CH_3, PBP-H and PBNP-H polymers.

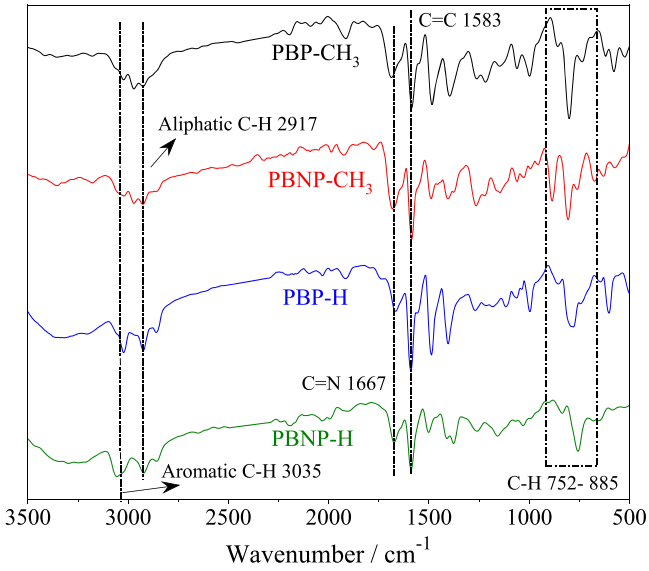

Fig. 4. FT-IR spectra of PBP-CH_3, PBNP-CH_3, PBP-H and PBNP-H membranes.

3.3. XRD

To further investigate the aggregation states of the four polymers, XRD was employed to obtain structural information. As shown in Fig. 5, all membranes exhibited a broad amorphous peak, indicating that they possessed amorphous structures. Notably, the PBNP-CH_3 membrane with binaphthyl units exhibited diffraction peaks at a higher angle compared to the PBP-CH_3 membrane with biphenyl units. The PBNP-H and PBP-H membranes showed the same phenomenon. According to Bragg's law ($n\lambda=2d\sin\theta$), higher diffraction angles correspond to smaller interplanar spacings, indicating tighter molecular packing in the binaphthyl-containing membranes. The binaphthyl moiety, composed of

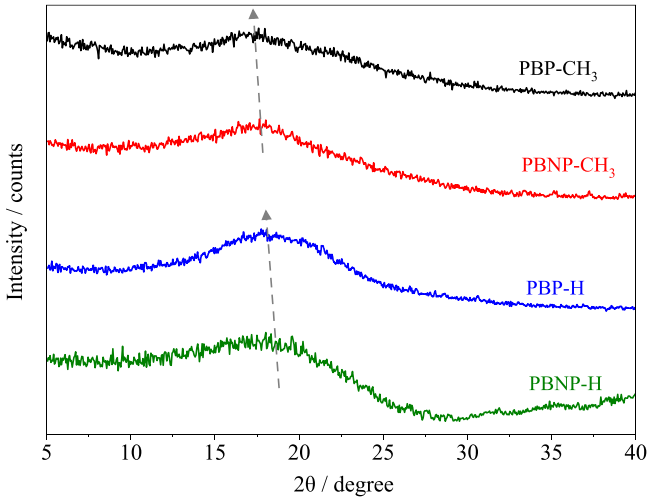

Fig. 5. XRD of PBP-CH_3, PBNP-CH_3, PBP-H and PBNP-H membranes.

fused aromatic rings, is larger and more rigid than the biphenyl unit, enhancing planarity and π-π stacking interactions between polymer chains. This leads to closer packing and reduced interlayer distances. In contrast, biphenyl units possess greater torsional freedom due to the single bond connecting the phenyl rings, resulting in less planarity and weaker π-π interactions. Consequently, membranes with biphenyl structures exhibit looser packing and larger interlayer spacings. These findings highlight that incorporating rigid and planar units like binaphthyl enhanced intermolecular interactions and packing density.

3.4. Chemical and thermal stabilities

The longevity and effectiveness of HT-PEMs are significantly dependent on the oxidative stability of the membranes. Roduner and colleagues have identified that the hydroperoxyl radical (HO_2•) and the hydroxyl radical (HO•) are primarily responsible for the degradation of aromatic polymers [47]. Oxidative stability assessments were performed by immersing the membranes in a Fenton's reagent solution composed of 3.0 wt% H_2O_2 and 4.0 ppm Fe^{2+} at 68 °C, as documented in previous studies [9,17,26]. Fig. 6 illustrates the percentage of weight retention for various membranes following the oxidation resistance trial, with inset photographs depicting the morphology of the membranes before and after the Fenton test. Upon examining the inset images within Fig. 6, it is evident that the PBP-CH_3, PBNP-CH_3, and PBNP-H membranes maintained their initial morphological characteristics after enduring 400 h of Fenton testing, with respective mass retention rates of 95.7 %, 99.5 %, and 90.5 %. The excellent chemical stability of above membranes could result from their rigid aromatic backbones and π-conjugated pyridine structures. Kallitsis et al. also observed that membranes featuring aromatic backbones with pendant pyridine groups exhibited outstanding oxidative resilience [48]. However, the PBP-H membrane fragmented after immersion in Fenton's reagent for just 25 h. This behavior is likely attributable to its unique chemical structure. The C—H bonds in the main chain linked to pyridine and binaphthalene moieties were reactive, making them susceptible to radical attack and subsequent removal. Additionally, it has been regarded that membranes with low viscosities are more prone to degradation in strongly oxidative environments. The relatively low viscosity (0.27 dL g^{-1}) of the PBP-H polymer may have further contributed to its poor chemical stability during the Fenton test. Consequently, the PBNP-CH_3 polymer enriched with acetylpyridine segments and dinaphthyl structures was anticipated to demonstrate enhanced chemical robustness.

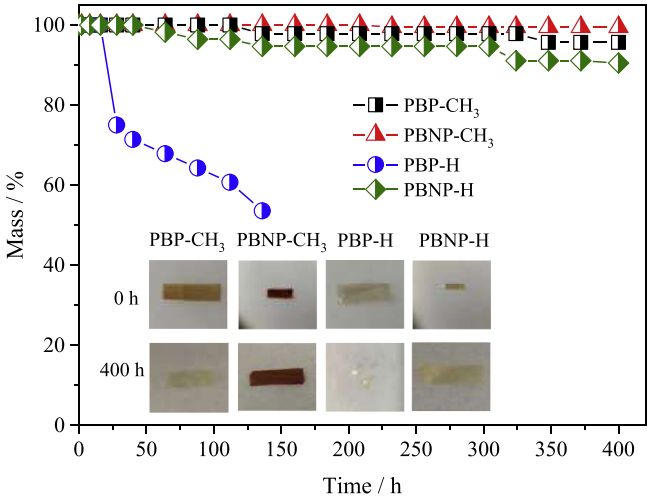

Fig. 6. Fenton test results of various membranes in 3 wt% H_2O_2 solution involving 4 ppm Fe^{2+} at 68 °C.

The TGA curves of PBP-CH_3, PBNP-CH_3, PBP-H, and PBNP-H in a nitrogen atmosphere are shown in Fig. 7. All the polymers exhibited excellent thermal stability below 200 °C. Notably, the membranes with dinaphthyl structures (PBNP-CH_3 and PBNP-H) demonstrated better thermal stability than those with biphenyl structures (PBP-CH_3 and PBP-H) up to 490 °C. Above 490 °C, the observed weight loss is attributed to the degradation of the aromatic main chain. The TGA results indicate that all the membranes are suitable for HT-PEMFC applications, as the operating temperature of HT-PEMFCs is typically below 200 °C [8].

3.5. Acid doping and swelling

The PA uptake of HT-PEM not only reflects the interaction between PA molecules and the membranes but also impacts their mechanical strength and ionic conductivity [17,26]. Table 1 lists ADC% and dimensional swelling of various membranes after immersion in 75 wt% and 85 wt% PA at 30 °C. The presence of dangling and freely rotating pyridine moieties within the polymer chains allowed the PBP-CH_3, PBNP-CH_3, PBP-H and PBNP-H membranes to interact with PA molecules through hydrogen bonding and acid-base interactions [43,49]. As a result, these membranes demonstrated superior PA uptake compared to OPBI. Among the membranes immersed in 75 and 85 wt% PA at 30 °C, the PBP-H membrane achieved the highest ADC%. Meanwhile, the PBP-CH_3 and PBP-H membranes exhibited remarkable PA absorption

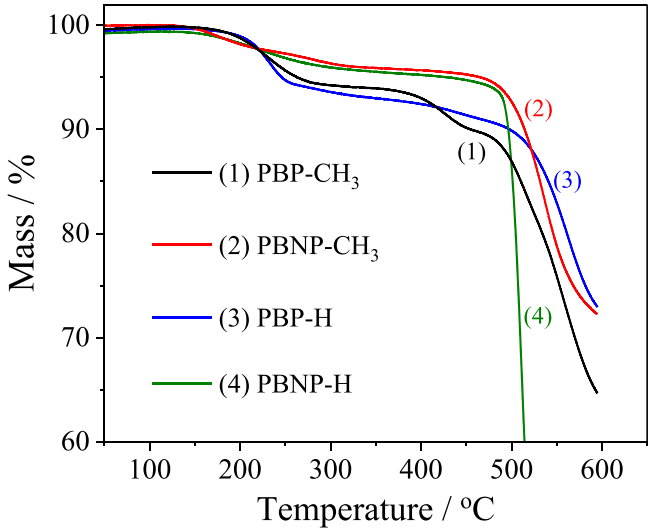

Fig. 7. TGA curves of PBP-CH_3, PBNP-CH_3, PBP-H and PBNP-H in N_2 atmosphere at a heating rate of 10 °C min^{-1}.

Table 1
Acid doping content and swellings of various membranes after immersing 85 wt % and 75 % PA solutions at 30 °C.

Membrane	85 wt% PA			75 wt% PA		
	ADC/%	S/%	V/%	ADC/%	S/%	V/%
PBP-CH_3	357.6	99.1	195.2	274.8	86.3	170.3
PBNP-CH_3	252.9	45.8	90.9	149.5	23.8	88.5
PBP-H	682.2	208.1	523.8	560.0	180.0	259.4
PBNP-H	282.2	59.6	143.8	172.0	38.2	65.5
OPBI	162.2	20.9	76.7	–	–	–

capabilities, likely attributed to the presence of biphenyl units. Additionally, Table 1 shows a decline in ADC% for each membrane corresponding to the reduction in the weight percentage of PA, a trend commonly observed in other HT-PEMs [28,31,50].

While a higher ADC% can facilitate proton transport, it may also induce deformation due to the plasticization effect of PA [17]. Typically, an increased ADC% in a membrane results in more significant swelling, both in area and volume, as illustrated in Table 1. For instance, after exposure to 85 wt% PA at 30 °C, the PBP-H membrane exhibited volume and area swellings of 208.1 % and 523.8 %, respectively, along with an ADC% of 682.2 %. In contrast, the PBNP-CH_3 and PBNP-H membranes demonstrated reduced swelling, primarily due to the rigidity and packing structure of the dinaphthyl units.

3.6. Mechanical properties

Outstanding mechanical strength is recognized as a pivotal element for both the assembly of MEA and the continuous functioning of HT-PEMFCs [6]. Fig. 8 illustrates the mechanical properties of the PBP-CH_3, PBNP-CH_3, PBP-H and PBNP-H membranes after doping in 85 wt% and 75 wt% PA solutions. PA-doped OPBI membranes were also

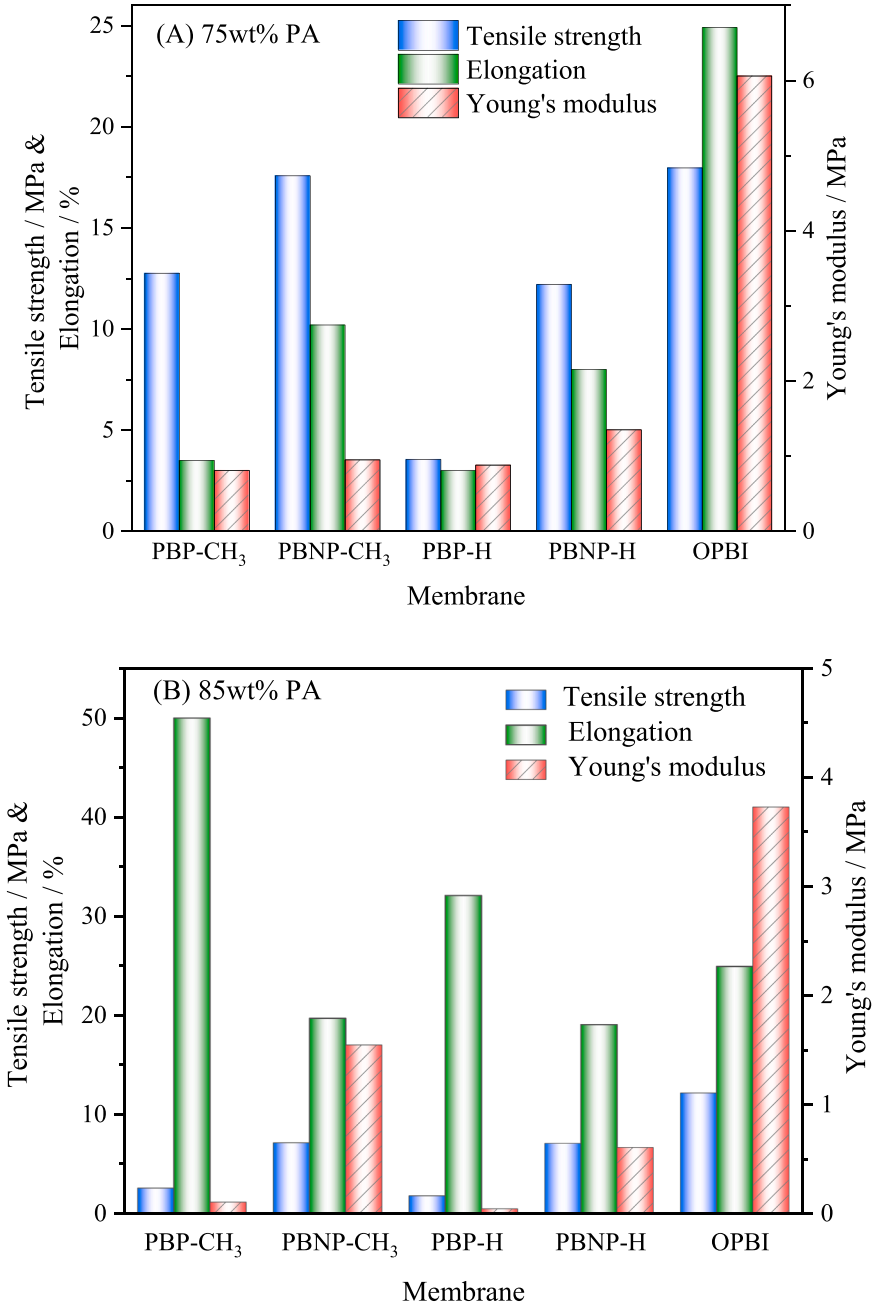

Fig. 8. Mechanical properties at RT of PBP-CH_3, PBNP-CH_3, PBP-H, PBNP-H and OPBI membranes after doped in (A) 75 wt% and (B) 85 wt% PA solutions.

included as a reference. As shown in Fig. 8A, the PBNP-CH_3 membrane with an ADC% of 149.5 % achieved the highest mechanical strength of 17.6 MPa among all the PA doped pyridine based membranes, which is similar to that of PA doped OPBI (18.0 MPa). The excellent mechanical integrity of the PBNP-CH_3/149.5 %PA membrane was likely attributed to its rigid dinaphthyl structure, fully aromatic polymer backbone and low swelling behavior. An increased PA uptake notably reduced the mechanical robustness of membranes due to the pronounced plasticizing influence of the PA molecules [26,46,48]. As a result, the PBP-H/560 % PA membrane with a biphenyl structure exhibited a reduced tensile strength of only 3.6 MPa. When doped in 85 wt% PA solution, both tensile strength and Young's modulus were decreased for each membrane due to the increased PA content. For example, the PBNP-CH_3/252.9 %PA membrane displayed tensile strength and Young's modulus of 7.2 MPa and 1.55 MPa, respectively. The tensile strengths for PBP-H/682.2 %PA and PBP-CH_3/357.6 %PA membranes with biphenyl units decreased to 2.6 MPa and 1.9 MPa, respectively. Thus, the PBNP-CH_3 membrane with its dinaphthyl structure and methyl group was more suitable for HT-PEMFCs due to its excellent mechanical stability.

3.7. Proton conductivity

Fig. 9 depicts the proton conductivities of the PA doped PBP-CH_3, PBNP-CH_3, PBP-H, and PBNP-H membranes over the temperature range of 100 °C to 180 °C. In general, increasing the temperature facilitates proton mobility, thereby enhancing the membrane's conductivity [26,27]. For example, the OPBI/162 %PA membrane exhibited conductivities of 7.4 mS cm^{-1} at 100 °C and 33.7 mS cm^{-1} at 180 °C. Moreover, the PBNP-CH_3/252.9 %PA membrane demonstrated conductivities of 33.1 mS cm^{-1} at 100 °C and 73.2 mS cm^{-1} at 180 °C. Regarding the PBP-H/682.2 % PA membrane, it exhibited the highest conductivity of 91.2 mS cm^{-1} at 120 °C among all the PA-doped membranes, a result clearly stemming from its superior ADC%. As previously documented, the enhancement of conductivity can be attributed to the formation of extensive and dynamic networks of hydrogen bonds, as well as channels that facilitate proton transport within PA-doped membranes [12]. However, it should be noted that both PBP-H/682.2 %PA and PBP-CH_3/357.6 %PA membranes could not be employed in HT-PEMFCs because they suffered significant deformation at elevated temperatures. Compared to HT-PEMs with high conductivities in literature, the PBNP-H/282.2 %PA membrane exhibited comparable or slightly lower values. For example, Shi et al. previously reported that the 0.5 % TPB-PBAP/326 %PA membrane reached a conductivity of 90 mS cm^{-1} [51]. Jana et al. reported that the Ph(CF_3)-PyOPBI/22.18PA exhibited a conductivity of 78 mS cm^{-1} at 180 °C [23], while the brominated polyphenylene oxide crosslinked pyridine-bridged-oxypolybenzimidazole with an acid doping level of 18 displayed the highest conductivity of 120 mS cm^{-1} at 180 °C [22].

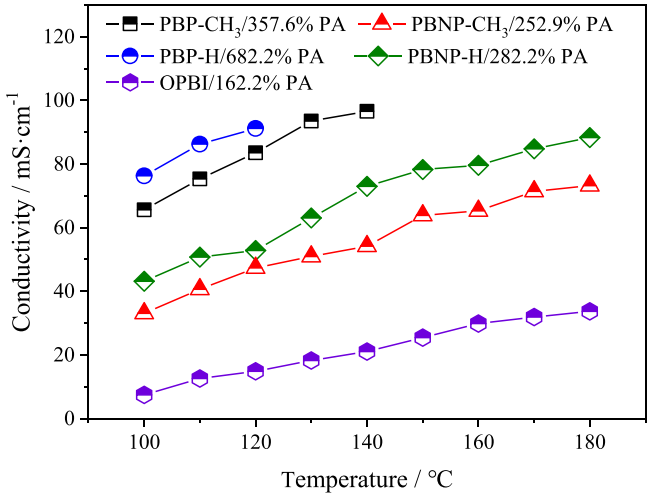

Fig. 9. Proton conductivities of PA doped various membranes as a function of temperature.

3.8. Fuel cell performance

In addition to their role in proton conduction, PA molecules doped into membranes can lead to plasticization and reduced tensile strength [6,9]. Therefore, striking a balance between proton conductivity and mechanical integrity is essential for PA doped HT-PEMs. Considering the overall physicochemical properties, the PBNP-CH_3/252.9 %PA membrane was selected for membrane electrode assembly (MEA) fabrication to evaluate the performance of a single cell using H_2 and O_2 without external humidification or backpressure at elevated temperatures, as shown in Fig. 10. As the test temperature increased, the cell performance improved, primarily due to enhanced proton conductivity and accelerated reaction kinetics [9,13]. For example, the peak power density of the cell increased from 434 mW cm^{-2} at 120 °C to 842 mW cm^{-2} at 160 °C, reachinig 1047 mW cm^{-2} at 200 °C. Notably, this H_2—O_2 peak power density of the PBNP-CH_3/252.9 %PA membrane was in a high level among previously reported values. For instance, the PTP-C5/202 %PA membrane achieved a H_2-air peak power density of 676 mW cm^{-2} at 210 °C [9], while the BA-a/PBI membrane reached a peak power density of 690 mW cm^{-2} at 160 °C [50].

4. Conclusions

To develop HT-PEMs with excellent overall performance, we synthesized robust, fully aromatic polymers containing pyridine groups through a one-step polymerization under mild conditions. Comparing with linear biphenyl structure, the bulky and twisted dinaphthyl structure was incorporated into pyridine-based polymers in order to enhance the dimensional stability and mechanical strength. Meanwhile, both 4-acetylpyridine and 4-pyridinecarboxaldehyde were employed as pyridine based monomers to investigate the structure-property relationships of membranes. PBP-CH_3 and PBNP-CH_3 polymers with –CH_3 group in main chain exhibited excellent solubility in NMP and $CHCl_3$, while PBP-H and PBNP-H polymers without –CH_3 group could dissolved in DMSO. Thus homogeneous membranes were fabricated via a simple solution-casting method. The successful synthesis of the above four polymers was confirmed by ^{1}H NMR and FT-IR spectroscopy, while SEM analysis revealed that all the membranes were dense and nonporous. XRD results indicated that incorporating rigid and planar units of binaphthyl enhanced intermolecular interactions and packing density. Fenton test

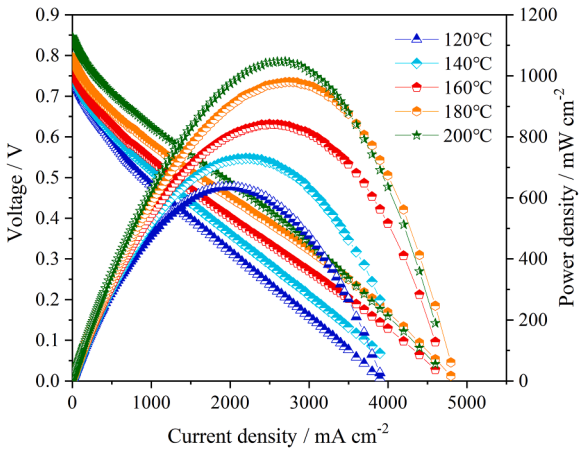

Fig. 10. Performance of fuel cell integrated with the PBNP-CH_3/252.9 %PA membrane under H_2 and O_2 without any humidification or backpressure.

and TGA results revealed that the prepared PBNP-CH_3 and PBNP-H membranes possessed good chemical resistance to radicals and thermal stability. Consequently, the PBNP-CH_3/252.9 %PA membrane was selected for fuel cell testing due to its high tensile strength of 7.2 MPa and good proton conductivity of 73.2 mS cm^{-1} at 180 °C. The H_2–O_2 HT-PEMFC using this membrane achieved peak power densities of 842 mW cm^{-2} at 160 °C and 1047 mW cm^{-2} at 200 °C without external humidification or backpressure. In summary, this study provides excellent membrane materials for high-temperature PEM fuel cells.

Declaration of competing interest

The authors declare that they have no known competing financial interests or personal relationships that could have appeared to influence the work reported in this paper.

Acknowledgements

We gratefully acknowledge the Fundamental Research Funds for the Central Universities of China (N2005026), Natural Science Foundation of Liaoning Province (2020-MS-087) and National Natural Science Foundation of China (52403273).

References

[1] F. Rahim Malik, H.-B. Yuan, J.C. Moran, N. Tippayawong, Overview of hydrogen production technologies for fuel cell utilization, Eng. Sci. Technol. 43 (2023) 101452, https://doi.org/10.1016/j.jestch.2023.101452.
[2] D. Shindell, C.J. Smith, Climate and air-quality benefits of a realistic phase-out of fossil fuels, Nature 573 (2019) 408–411, https://doi.org/10.1038/s41586-019-1554-z.
[3] A. Mancino, C. Menale, F. Vellucci, M. Pasquali, R. Bubbico, PEM fuel cell applications in road transport, Energies 16 (2023) 6129, https://doi.org/10.3390/en16176129.
[4] J. Xu, C. Zhang, Z. Wan, X. Chen, S.H. Chan, Z. Tu, Progress and perspectives of integrated thermal management systems in PEM fuel cell vehicles: a review, Renew. Sust. Energ. Rev. 155 (2022) 111908, https://doi.org/10.1016/j.rser.2021.111908.
[5] L. Huang, H. Xu, B. Jing, Q. Li, W. Yi, S. Sun, Progress of Pt-based catalysts in proton-exchange membrane fuel cells: a review, J. Electrochem. 28 (2022) 2108061, https://doi.org/10.13208/j.electrochem.210806.
[6] R. Haider, Y. Wen, Z.-F. Ma, D.P. Wilkinson, L. Zhang, X. Yuan, S. Song, J. Zhang, High temperature proton exchange membrane fuel cells: progress in advanced materials and key technologies, Chem. Soc. Rev. 50 (2021) 1138–1187, https://doi.org/10.1039/d0cs00296h.
[7] X. Guo, Y. Guo, J. Wang, B. Xiao, Y. Cao, C. Wu, Thermodynamic analysis and optimization of a novel hybrid system using thermoacoustic cycle to harvest waste heat of high temperature PEMFC, Energy Conv. Manag. 260 (2022) 115572, https://doi.org/10.1016/j.enconman.2022.115572.
[8] H. Guo, Z. Li, H. Pei, P. Sun, L. Zhang, P. Li, X. Yin, Stable branched polybenzimidazole high temperature proton exchange membrane: crosslinking and pentaphosphonic-acid doping lower fuel permeability and enhanced proton transport, J. Membr. Sci. 644 (2022) 120092, https://doi.org/10.1016/j.memsci.2021.120092.
[9] X. Che, L. Wang, T. Wang, J. Dong, J. Yang, The effect of grafted alkyl side chains on the properties of poly(terphenyl piperidinium) based high temperature proton exchange membranes, Ind. Chem. Mater. 1 (2023) 516–525, https://doi.org/10.1039/d3im00064h.
[10] Chinese Society of Electrochemistry, The top ten scientific questions in electrochemistry, J. Electrochem. 30 (1) (2024) 2024121, https://doi.org/10.61558/2993-074X.3444.
[11] S.S. Araya, F. Zhou, V. Liso, S.L. Sahlin, J.R. Vang, S. Thomas, X. Gao, C. Jeppesen, S.K. Kær, A comprehensive review of PBI-based high temperature PEM fuel cells, Int. J. Hydrog. Energy 41 (2016) 21310–21344, https://doi.org/10.1016/j.ijhydene.2016.09.024.
[12] Y. Jin, T. Wang, X. Che, J. Dong, R. Liu, J. Yang, New high-performance bulky N-heterocyclic group functionalized poly(terphenyl piperidinium) membranes for HT-PEMFC applications, J. Membr. Sci. 641 (2022) 119884, https://doi.org/10.1016/j.memsci.2021.119884.
[13] J. Chen, J.J. Bailey, L. Britnell, M. Perez-Page, M. Sahoo, Z. Zhang, A. Strudwick, J. Hack, Z. Guo, Z. Ji, P. Martin, D.J.L. Brett, P.R. Shearing, S.M. Holmes, The performance and durability of high-temperature proton exchange membrane fuel cells enhanced by single-layer graphene, Nano Energy 93 (2022) 106829, https://doi.org/10.1016/j.nanoen.2021.106829.
[14] G. Nawn, G. Pace, S. Lavina, K. Vezzù, E. Negro, F. Bertasi, S. Polizzi, V. Di Noto, Interplay between composition, structure, and properties of new H3PO4-Doped PBI4N–HfO2 nanocomposite membranes for high-temperature proton exchange membrane fuel cells, Macromolecules. 48 (2014) 15–27, https://doi.org/10.1021/ma5018956.
[15] L. Vilčiauskas, M.E. Tuckerman, G. Bester, S.J. Paddison, K.-D. Kreuer, The mechanism of proton conduction in phosphoric acid, Nat. Chem. 4 (2012) 461–466, https://doi.org/10.1038/NCHEM.1329.
[16] J.S. Wainright, J.T. Wang, D. Weng, R.F. Savinell, M. Litt, Acid-doped Polybenzimidazoles: a new polymer electrolyte, J. Electrochem. Soc. 142 (2019) L121–L123, https://doi.org/10.1149/1.2044337.
[17] D. Aili, J. Yang, K. Jankova, D. Henkensmeier, Q. Li, From polybenzimidazoles to polybenzimidazoliums and polybenzimidazolides, J. Mater. Chem. A 8 (2020) 12854–12886, https://doi.org/10.1039/d0ta01788d.
[18] T.-C. Xu, C.-S. Wang, Z.-Y. Hu, J.-J. Zheng, S.-H. Jiang, S.-J. He, H.-Q. Hou, High strength and stable proton exchange membrane based on perfluorosulfonic acid/polybenzimidazole, Chin. J. Polym. Sci. 40 (2022) 764–771, https://doi.org/10.1007/s10118-022-2708-2.
[19] F. Liu, S. Wang, H. Chen, J. Li, X. Wang, T. Mao, Z. Wang, The impact of poly (ionic liquid) on the phosphoric acid stability of polybenzimidazole-base HT-PEMs, Renew. Energy 163 (2021) 1692–1700, https://doi.org/10.1016/j.renene.2020.09.136.
[20] X. Zhang, Q. Liu, L. Xia, D. Huang, X. Fu, R. Zhang, S. Hu, F. Zhao, X. Li, X. Bao, Poly(2,5-benzimidazole)/sulfonated sepiolite composite membranes with low phosphoric acid doping levels for PEMFC applications in a wide temperature range, J. Membr. Sci. 574 (2019) 282–298, https://doi.org/10.1016/j.memsci.2018.12.085.
[21] S. Maity, T. Jana, Soluble polybenzimidazoles for pem: synthesized from efficient, inexpensive, readily accessible alternative tetraamine monomer, Macromolecules. 46 (2013) 6814–6823, https://doi.org/10.1021/ma401404c.
[22] R.Natak Harilal, P.C. Ghosh, T. Jana, Cross-linked polybenzimidazole membrane for PEM fuel cells, ACS Appl. Polym. Mater. 2 (8) (2020) 3161–3170, https://doi.org/10.1021/acsapm.0c00350.
[23] A.Shukla Harilal, P.C. Ghosh, T. Jana, Pyridine-bridged polybenzimidazole for use in high-temperature pem fuel cells, ACS Appl. Energy. Mater. 4 (2021) 1644–1656, https://doi.org/10.1021/acsaem.0c02821.
[24] A.Shukla Harilal, P.C. Ghosh, T. Jana, Copolymers of pyridine-bridged polybenzimidazole for the use in high temperature PEM fuel cell, Eur. Polym. J 177 (2021) 111445, https://doi.org/10.1016/j.eurpolymj.2022.111445.
[25] R.Bhattacharyya Harilal, A. Shukla, P.C. Ghosh, T. Jana, Rational design of microporous polybenzimidazole framework for efficient proton exchange membrane fuel cells, J. Mater. Chem. A 10 (20) (2022) 11074–11091, https://doi.org/10.1039/d2ta00734g.
[26] Q. Li, J.O. Jensen, R.F. Savinell, N.J. Bjerrum, High temperature proton exchange membranes based on polybenzimidazoles for fuel cells, Prog. Polym. Sci. 34 (2009) 449–477, https://doi.org/10.1016/j.progpolymsci.2008.12.003.
[27] E. Qu, X. Hao, M. Xiao, D. Han, S. Huang, Z. Huang, S. Wang, Y. Meng, Proton exchange membranes for high temperature proton exchange membrane fuel cells: challenges and perspectives, J. Power Sources 533 (2022) 231386, https://doi.org/10.1016/j.jpowsour.2022.231386.
[28] J. Yang, J. Wang, C. Liu, L. Gao, Y. Xu, Q. Che, R. He, Influences of the structure of imidazolium pendants on the properties of polysulfone-based high temperature proton conducting membranes, J. Membr. Sci. 493 (2015) 80–87, https://doi.org/10.1016/j.memsci.2015.06.010.
[29] S. Wang, Q. Li, F. Wang, The effect of imidazolated PPO with different alkyl chains on its performance as a high temperature proton exchange membrane, Polym.-Plast. Tech. Mater. 59 (2020) 1473–1481, https://doi.org/10.1080/25740881.2020.1750650.
[30] W. Ma, C. Zhao, H. Lin, G. Zhang, J. Ni, J. Wang, S. Wang, H. Na, High-temperature water-free proton conducting membranes based on poly(arylene ether ketone) containing pendant quaternary ammonium groups with enhanced proton transport, J. Power Sources 196 (2011) 9331–9338, https://doi.org/10.1016/j.jpowsour.2011.08.003.
[31] C. Charalampopoulos, K.J. Kallitsis, C. Anastasopoulos, M.K. Daletou, S. G. Neophytides, A.K. Andreopoulou, J.K. Kallitsis, Crosslinked polymer electrolytes of high pyridine contents for HT-PEM fuel cells, Int. J. Hydrog. Energy 45 (2020) 35053–35063, https://doi.org/10.1016/j.ijhydene.2020.06.004.
[32] K.J. Kallitsis, R. Nannou, A.K. Andreopoulou, M.K. Daletou, D. Papaioannou, S. G. Neophytides, J.K. Kallitsis, Crosslinked wholly aromatic polyether membranes based on quinoline derivatives and their application in high temperature polymer electrolyte membrane fuel cells, J. Power Sources 379 (2018) 144–154, https://doi.org/10.1016/j.jpowsour.2018.01.034.
[33] D.A. Klumpp, Y. Zhang, P.J. Kindelin, S. Lau, Superacid-catalyzed reactions of pyridinecarboxaldehydes, Tetrahedron. 62 (2006) 5915–5921, https://doi.org/10.1016/j.tet.2006.04.022.
[34] A.R. Cruz, M.C.G. Hernandez, M.T. Guzmán-Gutiérrez, M.G. Zolotukhin, S. Fomine, S.L. Morales, H. Kricheldorf, E.S. Wilks, J. Cárdenas, M. Salmón, Precision synthesis of narrow polydispersity, ultrahigh molecular weight linear aromatic polymers by A2 + B2 nonstoichiometric step-selective polymerization, Macromolecules. 45 (2012) 6774–6780, https://doi.org/10.1021/ma301691f.
[35] L.I. Olvera, M.T. Guzmán-Gutiérrez, M.G. Zolotukhin, S. Fomine, J. Cárdenas, F. A. Ruiz-Trevino, D. Villers, T.A. Ezquerra, E. Prokhorov, Novel high molecular weight aromatic fluorinated polymers from One-Pot, metal-free step polymerizations, Macromolecules. 46 (2013) 7245–7256, https://doi.org/10.1021/ma401306s.
[36] V.M. Velasco, M.G. Zolotukhin, M.T. Guzmán-Gutiérrez, S.L. Morales, S. Fomine, M.P. Carreón-Castro, M. Salmón, U. Scherf, Novel aromatic polymers with pentafluorophenyl pendent groups, Macromolecules. 41 (2008) 8504–8512, https://doi.org/10.1021/ma8016162.

[37] Y. Jin, T. Wang, X. Che, J. Dong, Q. Li, J. Yang, Poly(arylene pyridine)s: new alternative materials for high temperature polymer electrolyte fuel cells, J. Power Sources 526 (2022) 231131, https://doi.org/10.1016/j.jpowsour.2022.231131.
[38] Y. Jin, T. Wang, W. Tang, N. Yu, J. Yang, High-performance Poly(biphenyl acetylpyridine) and Poly(ether ketone cardo) blend membranes for high-temperature polymer electrolyte membrane fuel cells, Macromol. Mater. Eng. 307 (2022) 2200300, https://doi.org/10.1002/mame.202200300.
[39] W.T. Gao, X.L. Gao, W.W. Gou, J.J. Wang, Z.H. Cai, Q.G. Zhang, A.M. Zhu, Q.L. Liu, High-performance tetracyclic aromatic anion exchange membranes containing twisted binaphthyl for fuel cells, J. Membr. Sci. 655 (2022) 120578, https://doi.org/10.1016/j.memsci.2022.120578.
[40] H. Zhang, X. He, H. Feng, C. Li, M. Li, A poly(binaphthyl-co-terphenyl quinuclidinium) anion exchange membrane with excellent alkaline stability and anion conductivity, J. Mater. Chem. A 12 (2024) 23570, https://doi.org/10.1039/d4ta03241a.
[41] W. Zhang, S. Chen, D. Chen, Z. Ye, Sulfonated Binaphthyl-Containing Poly(arylene ether ketone)s with rigid backbone and excellent film-forming capability for proton exchange membranes, Polymers 10 (2018) 1287, https://doi.org/10.3390/polym10111287.
[42] T. Mu, W. Tang, Y. Jin, X. Che, J. Liu, J. Yang, Ether-Free Poly(p-terphenyl-co-acetylpyridine) membranes with different thicknesses for vanadium redox flow batteries, ACS Appl. Energ. Mater. 5 (2022) 11713–11722, https://doi.org/10.1021/acsaem.2c02216.
[43] B. Zhao, Z. Zhang, J. Zhang, L. Wang, T. Wang, J. Dong, C. Xu, J. Yang, Long side-chain N-heterocyclic cation based ionic liquid grafted poly(terphenyl piperidinium) membranes for anion exchange membrane fuel cell applications, Polymer 286 (2023) 126404, https://doi.org/10.1016/j.polymer.2023.126404.
[44] J. Yang, H. Jiang, J. Wang, Y. Xu, C. Pan, Q. Li, R. He, Dual cross-linked polymer electrolyte membranes based on poly(aryl ether ketone) and poly(styrene-vinylimidazole-divinylbenzene) for high temperature proton exchange membrane fuel cells, J. Power Sources 480 (2020) 228859, https://doi.org/10.1016/j.jpowsour.2020.228859.
[45] R. Lv, S. Jin, L. Li, Q. Wang, L. Wang, J. Wang, J. Yang, The influence of comonomer structure on properties of poly(aromatic pyridine) copolymer membranes for HT-PEMFCs, J. Membr. Sci. 701 (2024) 122703, https://doi.org/10.1016/j.memsci.2024.122703.
[46] T. Wang, Y. Jin, T. Mu, T. Wang, J. Yang, Tröger's base polymer blended with poly (ether ketone cardo) for high temperature proton exchange membrane fuel cell applications, J. Membr. Sci. 654 (2022) 120539, https://doi.org/10.1016/j.memsci.2022.120539.
[47] G. Hübner, E. Roduner, EPR investigation of HO/radical initiated degradation reactions of sulfonated aromatics as model compounds for fuel cell proton conducting membranes, J. Mater. Chem. 9 (1999) 409–418, https://doi.org/10.1039/a807129b.
[48] M. Geormezi, V. Deimede, J.K. Kallitsis, S. Neophytides, Polymer blends based on copolymers bearing both side and main chain pyridine units as proton exchange membranes for high temperature fuel cells, J. Membr. Sci. 396 (2012) 57–66, https://doi.org/10.1016/j.memsci.2011.12.039.
[49] Y. Jin, R. Liu, X. Che, T. Wang, J. Yang, New high temperature polymer electrolyte membranes based on Poly(ethylene imine) crosslinked Poly(ether ketone cardo), J. Electrochem. Soc. 168 (2021) 054524, https://doi.org/10.1149/1945-7111/ac009c.
[50] L. Wang, Z. Liu, Y. Liu, L. Wang, Crosslinked polybenzimidazole containing branching structure with no sacrifice of effective N-H sites: towards high-performance high-temperature proton exchange membranes for fuel cells, J. Membr. Sci. 583 (2019) 110–117, https://doi.org/10.1016/j.memsci.2019.04.030.
[51] N. Shi, G. Wang, Q. Wang, L. wang, Q. Li, J. Yang, Acid doped branched poly (biphenyl pyridine) membranes for high temperature proton exchange membrane fuel cells and vanadium redox flow batteries, Chem. Eng. J 489 (2024) 151121, https://doi.org/10.1016/j.cej.2024.151121.